atoms

MDPI

Article

Probing Atomic 'Quantum Grating' by Collisions with Charged Particles

Bennaceur Najjari [1], Shaofeng Zhang [1], Xinwen Ma [1] and Alexander B. Voitkiv [2,*]

[1] Institute of Modern Physics, Chinese Academy of Sciences, Lanzhou 730000, China
[2] Institute for Theoretical Physics I, Heinrich-Heine-University of Düsseldorf, Universitätsstrasse 1, 40225 Düsseldorf, Germany
* Correspondence: alexander.voitkiv@tp1.uni-duesseldorf.de

Abstract: The wave function of an atom, which passed through a diffraction grating, is characterized by a regular space structure. Correspondingly, the interaction of another particle with this atom can be viewed as scattering on an 'atomic quantum grating' made of just a *single atom*. Probing this 'grating' by collisions with a charged projectile reveals few-body interference phenomena caused by the coherent contributions of its 'slits' to the transition amplitude (the superposition principle) and quantum entanglement of the particles involved. In particular, the spectra of electrons emitted from the atom in collisions with swift ions exhibit a pronounced interference pattern whose shape can be extremely sensitive to the collision velocity.

Keywords: quantum-grating; few-body interference; quantum entanglement; ion–atom collisions

check for updates

Citation: Najjari, B.; Zhang, S.; Ma, X.; Voitkiv, A.B. Probing Atomic 'Quantum Grating' by Collisions with Charged Particles. *Atoms* **2022**, *10*, 125. https://doi.org/10.3390/atoms10040125

Academic Editor: G. W. F. Drake

Received: 20 September 2022
Accepted: 17 October 2022
Published: 1 November 2022

Publisher's Note: MDPI stays neutral with regard to jurisdictional claims in published maps and institutional affiliations.

Copyright: © 2022 by the authors. Licensee MDPI, Basel, Switzerland. This article is an open access article distributed under the terms and conditions of the Creative Commons Attribution (CC BY) license (https://creativecommons.org/licenses/by/4.0/).

1. Introduction

One of the fundamental concepts of quantum physics is the wave–particle duality: all atomic objects exhibit both particle and wave properties. It was proposed by Louis de Broglie [1] in 1923. Since then, a number of experiments confirmed the wave nature of various atomic particles ranging from electrons [2,3] to huge molecules consisting of many thousands of atoms [4].

In most of these experiments, atomic particles were detected after passing through slits (a diffraction grating). In this phenomenon, which is essentially similar to the famous Young's double-slits interference of light [5], the coherent addition of the amplitudes for different quantum paths (the superposition principle) leads to interference in the detection probabilities, clearly demonstrating the wave-like behavior of the particles.

The diffraction gratings employed in these experiments were naturally macroscopic. Their microscopic analogues can be found in the atomic world. For instance, a diatomic molecule in processes, where its internal state does not change, may play essentially the same role as the Young's double slits in the interaction with light. Since interference effects in processes involving such molecules also arise when their internal state change, it is obvious that—despite their much smaller size—these microscopic 'slits' are associated with richer interference effects. Therefore, beginning with the work of [6,7], very significant efforts have been devoted to exploring various interference phenomena arising when particles interact with such molecules (see, e.g., [8–25]).

A qualitatively different type of microscopic 'grating' can be obtained by letting an atom to pass through a macroscopic diffraction grating. Indeed, the wave function of the atom acquires a periodic space structure. As a result, the interaction of another particle with this atom can be viewed as the scattering of the former on an object which can be called an 'atomic quantum grating'. Like its macroscopic counterpart, it possesses a periodic structure, which consists of stronger and weaker interacting parts corresponding to, respectively, larger and smaller values of the atomic probability density, but is made of

just a single atom. Thus, the structured probability amplitude of a single atom essentially plays now the role of a structured macroscopic piece of matter in usual gratings.

Recently, we considered the photoionization of atomic quantum grating [26,27]. Here, we explore some aspects of the interaction of an atomic quantum grating with swift charged projectiles. Effects caused by coherent contributions to the transition amplitude from different 'slits' of the quantum grating will be considered for elastic as well as inelastic collisions. It will be shown that they represent two- (and three-) particle interference phenomena for which both the superposition principle and quantum entanglement of the particles involved are of crucial importance [28–31].

Atomic units ($\hbar = m_e = |e| = 1$) are used throughout, except where otherwise stated.

2. General Consideration

Let an atom, which moves in the laboratory frame with a momentum $\mathbf{P}_a^i = (0, P_a^i, 0)$, pass through a macroscopic diffraction grating. The grating, which is at rest in the laboratory frame, is assumed to be located in the (x–z)–plane and consists of N_0 slits along the z direction (see Figure 1). The dimensions of the slits are a and b (along the z and x directions, respectively), and the period of the grating is d. For the moment, we choose the origin of our coordinate system to be placed in the middle of the diffraction grating (see Figure 1).

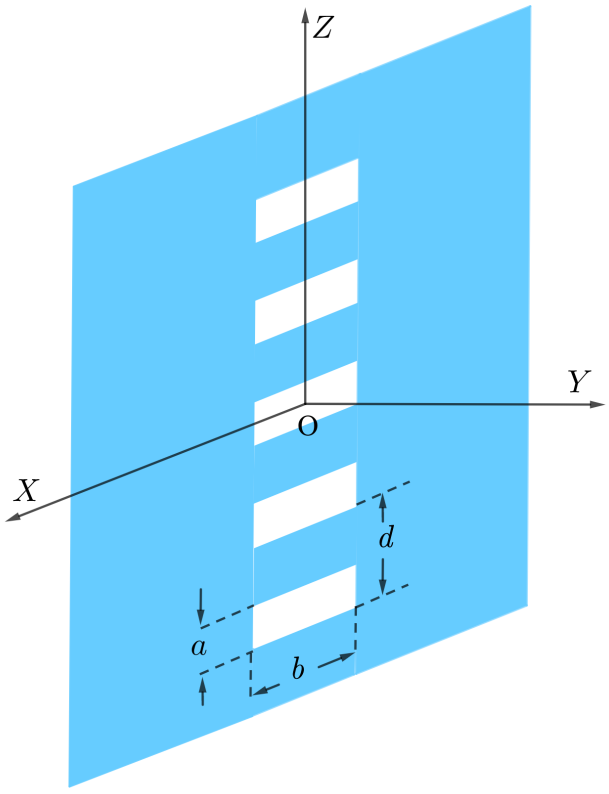

Figure 1. A diffraction grating with slits located in the x–z plane, a and b are the slit dimensions and d is the period of the grating.

Before the diffraction grating, the wavefunction $\psi(\mathbf{R}_a, \mathbf{r}_e, t)$ of the incident atom is given by

$$\begin{aligned} \psi(\mathbf{R}_a, \mathbf{r}_e, t) &= \psi_{in}(\mathbf{R}_a, \mathbf{r}_e, t) \\ &= A \exp(i\,\mathbf{P}_a^i \cdot \mathbf{R}_a - i\,E_a^i t)\,\phi_i(\mathbf{r}_e - \mathbf{R}_N), \end{aligned} \tag{1}$$

where A is the normalization constant, $\mathbf{R}_a = (X_a, Y_a, Z_a)$, where $X_a = R_a \sin\vartheta_{\mathbf{R}_a} \cos\varphi_{\mathbf{R}_a}$, $Y_a = R_a \sin\vartheta_{\mathbf{R}_a} \sin\varphi_{\mathbf{R}_a}$ and $Z_a = R_a \cos\vartheta_{\mathbf{R}_a}$, is the coordinate of the atomic center-of-mass, and $\mathbf{r}_e$ and $\mathbf{R}_N$ are the position vectors of the atomic electron and the atomic nucleus,

respectively (all these coordinates are given with respect to the origin). Furthermore, ϕ_i is the initial atomic internal state with an energy ε_i and $E_a^i = \varepsilon_i + {\mathbf{P}_a^i}^2/2M_A$ is the total initial energy of the atom where M_A is the atomic mass.

Using the Huygens–Fresnel principle, we obtain that, after the passage through the grating, the wave function of the atom at asymptotically large distances ($R_a \gg \max\{N_0\, d,\, b\}$) can be approximated as

$$\begin{aligned}\psi(\mathbf{R}_a, \mathbf{r}_e, t) &= \psi_{diff}(\mathbf{R}_a, \mathbf{r}_e, t)\\ &= \frac{4A}{R_a}\exp(i\,P_a^i\,R_a - i\,E_a^i t)\\ &\quad\times\frac{\sin\left(\frac{P_a^i\,a\,Z_a}{2\,R_a}\right)}{P_a^i\,\frac{Z_a}{R_a}}\;\frac{\sin\left(\frac{P_a^i\,b\,X_a}{2\,R_a}\right)}{P_a^i\,\frac{X_a}{R_a}}\\ &\quad\times\frac{\sin\left(N_0\frac{P_a^i\,d\,Z_a}{2\,R_a}\right)}{\sin\left(\frac{P_a^i\,d\,Z_a}{2\,R_a}\right)}\,\phi_i(\mathbf{r}_e - \mathbf{R}_N).\end{aligned} \tag{2}$$

We note that the application of the Huygens–Fresnel principle to describe (optical) diffraction is known to yield excellent results provided the wavelength of light is smaller than $\min\{a, b\}$. In what follows, we assume that $P_a^i \simeq 10 - 100$ a.u. and the wavelength of the atom, $\lambda_a^i = 1/P_a^i$, will certainly be much smaller than $\min\{a, b\}$, which enables one to expect that (2) represents a good approximation for the wave function at asymptotically large distances between the atom and the grating ($R_a \gg \max\{N_0\, d,\, b\}$).

As it follows from (2), the wave function of the atom acquired—due to diffraction—a regular space structure. This structure can be unveiled in many ways. In what follows, we consider how it can be probed by letting the atom interact with a projectile which we take here as a point-like charged particle (an electron or a bare nucleus).

Assuming that the energy of the projectile is sufficiently high, we approximate its initial and final states by plane waves

$$\begin{aligned}\Phi_i(\mathbf{R}_p, t) &= \frac{1}{\sqrt{V_p}}\exp(i\,\mathbf{p}_p^i\cdot\mathbf{R}_p - i\,\varepsilon_p^i\,t)\\ \Phi_f(\mathbf{R}_p, t) &= \frac{1}{\sqrt{V_p}}\exp(i\,\mathbf{p}_p^f\cdot\mathbf{R}_p - i\,\varepsilon_p^f\,t).\end{aligned} \tag{3}$$

Here, $\mathbf{R}_p$ is the position vector of the projectile with respect to the origin, $\mathbf{p}_p^i$ and $\varepsilon_p^i = {\mathbf{p}_p^i}^2/2M_p$ ($\mathbf{p}_p^f$ and $\varepsilon_p^f = {\mathbf{p}_p^f}^2/2M_p$) are the initial (final) momentum and energy, respectively, of the projectile in the laboratory frame, M_p is its mass, and V_p is the normalization volume.

Assuming that the momentum of the atom after the collision is detected, we take its final state as a product of a plane wave, which describes the motion of its center-of-mass, and a final internal state of the atom ϕ_f with an energy ε_f,

$$\psi_f(\mathbf{R}_a, \mathbf{r}_e, t) = \frac{\exp(i\,\mathbf{P}_a^f\cdot\mathbf{R}_a - i\,E_a^f t)}{\sqrt{V_a}}\phi_f(\mathbf{r}_e - \mathbf{R}_N), \tag{4}$$

where $\mathbf{P}_a^f$ and $E_a^f = \varepsilon_f + {\mathbf{P}_a^f}^2/2\,M_A$ are the final momentum and energy of the atom, respectively, and V_a is the normalization volume. The state ϕ_f can be either a bound or continuum state; the latter case corresponds to ionization.

In the first order of perturbation theory, which normally represents a reasonable approximation provided $Z_p/v \ll 1$ where Z_p is the projectile charge and v is the collision velocity, the transition amplitude reads

$$S_{fi} = -i \int_{-\infty}^{+\infty} dt \ \langle \Psi_f(t) \mid \hat{W} \mid \Psi_i(t) \rangle. \tag{5}$$

Here, $\Psi_i(t) = \psi_{diff}(\mathbf{R}_a, \mathbf{r}_e, t)\, \Phi_i(\mathbf{R}_p, t)$ and $\Psi_f(t) = \psi_f(\mathbf{R}_a, \mathbf{r}_e, t)\, \Phi_f(\mathbf{R}_p, t)$ are the initial and final states, respectively, of the non-interacting "atom + projectile" system and $\hat{W} = -Z_p/|\mathbf{r}_e - \mathbf{R}_p| + Z_p Z_N/|\mathbf{R}_N - \mathbf{R}_p|$, where Z_p (Z_N) is the charge of the projectile (the atomic nucleus), which is the interaction between them.

Let the target and projectile beams cross at a distance D from the grating. At this distance, a single target atom is localized (along the z axis) within a spot whose size Δ_z can be estimated from the form of the state (2) and is roughly given by $\Delta_z \simeq D/P_a^i\, a \sim D\, \lambda_a^i/a$. Taking $D \simeq 200$–1000 mm, $a \simeq 10^{-3}$–0.1 mm and $P_a^i \simeq 10$–100 a.u. we obtain $\Delta_z \sim 10^{-7}$–10^{-3} mm. This value is much smaller than the size $L_z = N_0\, d$ ($\simeq 10^{-2}$–1 mm) of the macroscopic grating along the z axis. Comparing Δ_z and L_z, we see that the typical size of the target spot, produced by all target atoms passed through the grating, is essentially determined by $N_0\, d \sim 10^{-2}$–1 mm, and thus is much smaller than the distance D.

A similar consideration shows that for a typical size of the target spot Δ_x along the x axis, one obtains $\Delta_x \simeq \frac{a}{b}\, \Delta_z$ and, assuming $b \simeq a$, one has $\Delta_x \sim 10^{-7}$–10^{-3} mm.

Using the above estimates and also noting that the diameter of the projectile beam in the collisional experiments is typically of the order of 1 mm (see, e.g., [32]), we obtain that each dimension of the interaction volume (the space volume where the beams cross) is much smaller than the distance D between its center and the macroscopic diffraction grating.

Taking all this into account, it is convenient to introduce a new coordinate system which also rests in the laboratory frame but whose origin is placed in the center of the interaction volume. The new (primed) and old (unprimed) coordinates of the particles are related by $\mathbf{R}'_a = \mathbf{R}_a - \mathbf{D}$, $\mathbf{R}'_p = \mathbf{R}_p - \mathbf{D}$, $\mathbf{r}'_e = \mathbf{r}_e - \mathbf{D}$, $\mathbf{R}'_N = \mathbf{R}_N - \mathbf{D}$, where $\mathbf{D} = (0, D, 0)$.

Using the new coordinates and performing the integrations over the interaction volume and time in (5), we obtain

$$\begin{aligned} S_{fi} &= 2^6\, \pi^3\, A\, i\, \delta((E_a^f + \varepsilon_p^f) - (E_a^i + \varepsilon_p^i)) \\ &\times \frac{\langle \phi_f(\boldsymbol{\xi}) \mid \exp(i\mathbf{q}\cdot\boldsymbol{\xi}) \mid \phi_i(\boldsymbol{\xi}) \rangle}{q^2}\, F_b(q_x - P_{a,x}^f) \\ &\times \frac{\exp(i\, P_a^i\, D)}{D} \times \delta(P_a^i + q_y - P_{a,y}^f) \\ &\times \sum_n F_a(q_z - P_{a,z}^f - P_a^i\, d\, n/D), \end{aligned} \tag{6}$$

where $\boldsymbol{\xi} = \mathbf{r}'_e - \mathbf{R}'_N$, $\mathbf{q} = (q_x, q_y, q_z) = \mathbf{p}_p^i - \mathbf{p}_p^f = (p_{p,x}^i - p_{p,x}^f, p_{p,y}^i - p_{p,y}^f, p_{p,z}^i - p_{p,z}^f)$ is the change in the projectile momentum (= the momentum transfer to the atom).

The functions F_α (where $\alpha = a, b$) are given by

$$F_\alpha(\kappa) = \frac{1}{\alpha} \int_{-L/2}^{+L/2} dl \ \ e^{i\,\kappa\, l} \ \ \frac{\sin\left(\frac{P_a^i \alpha}{2D}\, l\right)}{\frac{P_a^i \alpha}{2D}\, l}. \tag{7}$$

Here, L is the length of the interaction region (for simplicity, we assume that it is the same for both x and z directions). If $\frac{P_a^i \alpha}{D} L \gg 2\pi$, the function $F_\alpha(\kappa)$ takes on very simple form:

$$F_\alpha(\kappa) = \begin{cases} \pi; \ |\kappa| < \frac{P_a^i \alpha}{2D} \\ \pi/2; \ |\kappa| = \frac{P_a^i \alpha}{2D} \\ 0; \ |\kappa| > \frac{P_a^i \alpha}{2D} \ . \end{cases} \quad (8)$$

The conditions $L\frac{P_i a}{D} \gg 2\pi$ and $L\frac{P_i b}{D} \gg 2\pi$ hold for a very broad parameter range and we shall assume that they are fulfilled.

It follows from (6) and (8) that, along the x and z directions, there are uncertainties, $\Delta P_x = P_a^i b/D$ and $\Delta P_z = P_a^i a/D$, in the momentum balance in the collision. This is caused by the (uncontrolled) momentum exchange between the atom and the macroscopic diffraction grating resulting in uncertainty in the momentum of the atom passed through it. However, the energy balance in the collision does not possess an uncertainty because the macroscopic grating, which has essentially infinite (on the atomic scale) mass and is initially at rest, does not participate in the energy exchange.

3. Results and Discussion

3.1. Elastic Collisions with Electrons

Suppose that projectile electrons, incident along the x axis, are elastically scattered on Xe atoms, which passed through a diffraction grating and whose velocity is negligibly small compared to that of the electrons. We note that, because of the spherical symmetry of the atomic potential acting on the electron, the scattering possesses a cylindrical symmetry in the plane perpendicular to the x axis.

Figure 2 displays the elastic cross-section for 300 eV electrons, differential in the projectile scattering angle and the z component $P_{a,z}^f$ of the final atomic momentum. A clear interference pattern observed in the cross-section along $P_{a,z}^f$ is caused by the coherent addition of the contributions of the different 'slits' of the atomic quantum grating to the process of electron scattering.

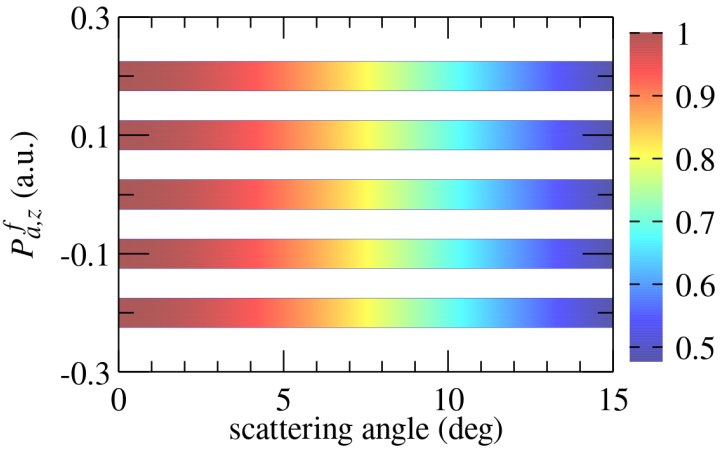

Figure 2. The differential cross-section for the elastic scattering of 300 eV electrons incident along the x axis on Xe atoms ($P_a^i = 100$ a.u.) passed through a diffraction grating with $a = b = d/2 = 0.1$ mm and $N_0 = 5$. $D = 200$ mm. The cross-section is given in relative units with its intensity ranging from 0.5 to 1. (The blank regions correspond to zero cross-section values).

3.2. Ionization in Collisions with Bare Ions

We now consider the collisions of atoms with bare ions resulting in atomic ionization. Assuming that the velocity of the atom before the collision, $v_a = P_a^i/M_a$, is much less than

the projectile velocity and the velocity of the emitted electron and using the transition amplitude (6), we obtain the following expression for the fully differential cross-section for atomic ionization

$$\begin{aligned}\frac{d\sigma}{d^3\mathbf{q}\; d^3\mathbf{P}_R\; d^3\mathbf{k}} &= 2^{12}\pi^4\; A^2\; \frac{Z_p^2}{v\; P_a^{i\,2}} \\ &\times \frac{|\langle \phi_{\mathbf{k}}(\boldsymbol{\xi}) \mid \exp(i\mathbf{q}\cdot\boldsymbol{\xi}) \mid \phi_i(\boldsymbol{\xi})\rangle|^2}{q^4} \\ &\times \delta(P_a^i + q_y - P_{R,y} - k_y) \\ &\times \delta(E_a^f + \varepsilon_p^f - E_a^i - \varepsilon_p^i) \\ &\times F_b^2(q_x - P_{R,x} - k_x) \\ &\times \sum_n F_a^2(B_n). \end{aligned} \tag{9}$$

Here, $\mathbf{P}_R = (P_{R,x}, P_{R,y}, P_{R,z})$ and $\mathbf{k} = (k_x, k_y, k_z)$ are the momenta of the target recoil ion and the emitted electron given in the laboratory frame, and $B_n = q_z - P_{R,z} - k_z - P_a^i\, d\, n/D$.

Since $M_A \gg m_e$ (m_e is the electron mass), one has $E_a^f - E_a^i \approx k^2/2 - \varepsilon_i$. Additionally, for collisions with $|\mathbf{q}| \ll |\mathbf{p}_i|$, one obtains $\varepsilon_p^i - \varepsilon_p^f = (\mathbf{p}_i^2 - \mathbf{p}_f^2)/2M_p = (\mathbf{p}_i - \mathbf{p}_f)(\mathbf{p}_i + \mathbf{p}_f)/2M_p \approx \mathbf{q}\cdot\mathbf{v}$. Therefore, the energy delta-function in (9) can be rewritten as $\frac{1}{v}\delta(q_\parallel - (k^2/2 - \varepsilon_i)/v)$, where $q_\parallel = \mathbf{q}\cdot\mathbf{v}/v$.

Let the projectile be incident along the z direction (we remind the reader that the slits in the diffraction grating are also along this direction, as can be seen in Figure 1). Integrating the cross-section (9) over $P_{R,x}$, $P_{R,y}$ and q_z, we obtain

$$\begin{aligned}\frac{d\sigma}{d^2\mathbf{q}_\perp dP_{R,z} d^3\mathbf{k}} &\sim \frac{Z_p^2}{v^2}\, \frac{|\langle \phi_{\mathbf{k}}(\boldsymbol{\xi}) \mid \exp(i\mathbf{q}_0\cdot\boldsymbol{\xi}) \mid \phi_i(\boldsymbol{\xi})\rangle|^2}{q_0^4} \\ &\times \sum_n F_a^2(B_n), \end{aligned} \tag{10}$$

where $\mathbf{q}_0 = (q_x, q_y, q_{min}) = (\mathbf{q}_\perp, q_{min})$ with $q_{min} = (k^2/2 - \varepsilon_i)/v$ and $B_n = q_{min} - P_{R,z} - k_z - P_a^i\, d\, n/D$.

The binary-encounter emission and electron capture to the projectile continuum belong to the most prominent features of ionization (see, e.g., ref. [33] and references therein). The former is a two-body ionization mechanism in which the momentum exchange in the collision occurs between the projectile and the electron, while the target nucleus/core is merely a spectator: $P_{R,x} \approx 0$, $P_{R,z} \approx 0$, $P_{R,y} \approx P_a^i$. In the latter, the emitted electron moves with a velocity $\mathbf{v}_e \approx \mathbf{v}$, i.e., together with the projectile but without forming a bound state with it.

Using the collision momentum balance along the z axis, $q_{min} \approx P_{R,z} + k_z$, and taking into account that $q_{min} = (k^2/2 + |\varepsilon_i|)/v$, we obtain $(k_z - v)^2 + k_{tr}^2 + (2|\varepsilon_i| - v^2) + 2vP_{R,z} \approx 0$, where $k_{tr} = \sqrt{k_x^2 + k_y^2}$ is the part of the electron momentum perpendicular to the projectile velocity. It follows from this equation that, provided $|\varepsilon_i| \approx v^2/2$, the above two features can be simultaneously present. Indeed, one obtains $k_z \approx v$, if $k_{tr} \approx 0$ and $P_{R,z} \approx 0$. Such an interesting situation is considered in Figure 3, where the cross-section $\frac{d^5\sigma}{d^2\mathbf{q}_\perp dP_{R,z} dk_z dk_\perp}$, taken at $P_{R,z} = q_x = q_y = 0$, is shown as a function of k_z and k_{tr} for the single ionization of atomic helium by proton projectiles.

As is well known [33], for the electron capture to the projectile continuum, the interaction between the projectile and the emitted electron is crucial. Since the first-order approximation neglects this interaction, the cross-section was calculated using the continuum-

distorted-wave eikonal-initial-state approach [34] which accounts for this interaction and yields a satisfactory description of this process.

The electron spectrum shown in Figure 3 exhibits a pronounced interference structure consisting of concentric rings. The center, the width, and the number of the rings are determined by the inequalities $B^- \leq (k_z - v)^2 + k_\perp^2 \leq B^+$, where $B^\pm = v^2 - 2|\varepsilon_i| + 2\,v\,P_{R,z} + 2\,v\,P_a^i\,\frac{d}{D}\,n \pm v\,P_a^i\,\frac{a}{D}$. This structure arises due to the coherent contributions to the emission from different parts of the atomic quantum grating, which strongly interfere in the cross-section. The number of the rings, their size, and even the relative intensity on them turn out to be extremely sensitive to the magnitude of the collision velocity.

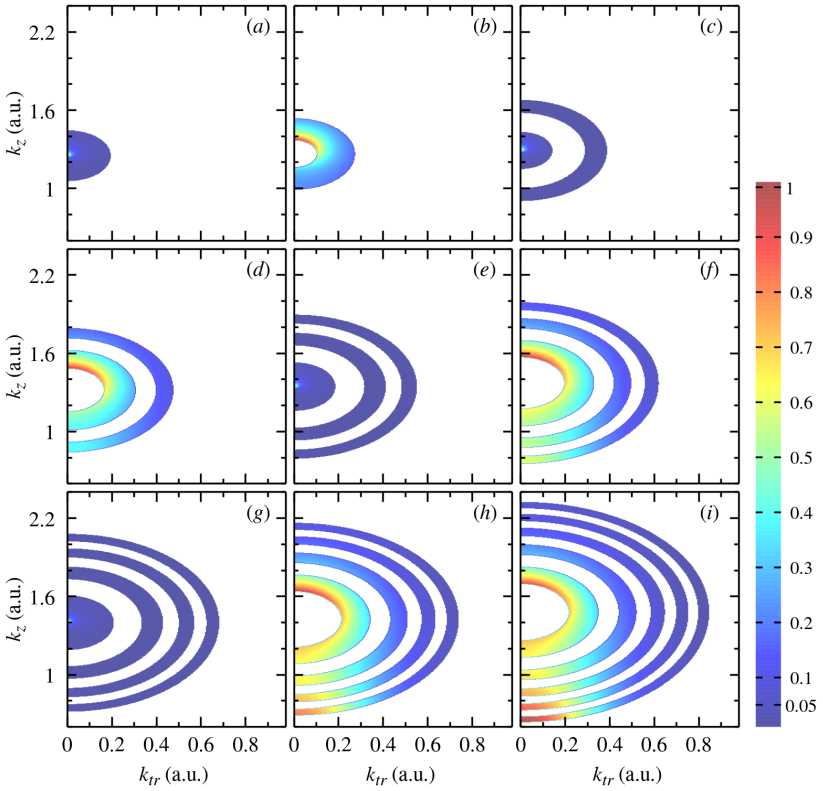

Figure 3. Spectra of electrons emitted from He atoms ($P_a^i = 50$ a.u., $v_a = P_a^i/M_a \approx 7 \times 10^{-3}$ a.u. $\to 0$, $\varepsilon_i = -0.9$ a.u.) passed through a diffraction grating ($a = b = d/2 = 0.1$ mm, $N_0 = 5$) in collisions with protons. $D = 200$ mm, $P_{R,z} = q_x = q_y = 0$. The collision velocity $v = f\,v_0$, where $v_0 = \sqrt{2|\varepsilon_i|}$ and $f = 0.93$ (**a**), 0.94 (**b**), 0.96 (**c**), 0.98 (**d**), 1 (**e**), 1.02 (**f**), 1.04 (**g**), 1.06 (**h**), and 1.1 (**i**). The spectra are given in relative units with their intensities ranging from 0 to 1. The blank regions correspond to zero cross-section values.

3.3. Collisions with Atomic Grating and the 'Standard' Interference

Interference patterns, which arise when massless or massive particles (photons, electrons, atoms, molecules, etc.) passed through a macroscopic diffraction grating are detected on a screen, belong to textbook examples of interference. They represent interference in the position coordinate space which arises because after the passage of the diffraction grating, the particle wave function acquires a periodic space structure with alternating maxima and minima in its absolute value (see, e.g., Equation (2)).

In the processes considered in the present paper, the collision 'converts' interference from the position coordinate space to the momentum space. Instead of the maxima and minima in the position space, now one deals with the 'allowed' and 'forbidden' momentum regions whose locations are described by the functions F_α (see Equations (6)–(10)).

3.4. Collisions with Atomic Grating as Two- and Three-Particle Interference Phenomena

Interference in electron elastic scattering and electron emission spectra (see Figures 2 and 3) originates in a periodic structure of the wave function of the target atom in the coordinate space (see Equation (2)). This makes the atom to behave effectively as a set of coherent centers of force that—according to the superposition principle—gives rise to interference.

However, the interference structures disappear if the integration is performed over the momentum of the recoiling atom (in the case of elastic scattering) or (in case of ionization) over that of the target recoil ion (or the projectile). In other words, interference is absent for any particle taken individually and only appears if the detection of the electron is accompanied by a coincidence measurement of the other particle(s). Thus, the fringes in Figure 2 (the rings in Figure 3) are in fact the signatures of two- (three-) particle interference phenomena arising provided the superposition principle and quantum entanglement of the particles involved 'act' together.

Two-photon (and multi-photon) interference and entanglement as well as their applications in quantum communication and computation have been intensively discussed (see, e.g., refs. [28,29]). More recently, two-particle interference was explored for atoms [30] and electrons [31]. The process of collisional ionization studied in the present paper represents—to our knowledge—the first considered example of three-particle interference where all involved particles are massive.

The process of atomic collisions unveils the information 'stored' in the atom. Unlike the wave function of a 'normal' atom, which carries information just about its momentum, internal state, and its binding energy, the wave function of an atom, which was formed by passing through a macroscopic diffraction grating, also contains the information about the parameters of the grating. According to the above-discussed results, the information about the grating (the size and number of slits, the distance between them), encoded in the state of the atom, can be decoded by measuring the cross-sections for elastic and inelastic collisions. It, however, remains to be seen whether the processes considered in the present paper (or their close analogues involving massive particles) can have any applications.

3.5. Atomic Grating and Other Basic Atomic Processes

Our estimates show that atomic quantum gratings can also profoundly manifest themselves in other basic atomic collision processes such as electron capture to a bound state of the projectile and projectile-electron loss where either the target or projectile passed before the collision through a macroscopic diffraction grating. Additionally, this is also the case for photoabsorption [26,27] and photon scattering.

3.6. Possible Experimental Verification

In our theoretical consideration of collisions with the atomic quantum grating, we assumed that the initial and final states of the projectile are plane waves and that the collision results in the 'collapse' of the wave function of the atomic quantum grating onto a plane wave. In other words, it is assumed that the projectile velocity, the momentum of the target (or the momenta of the target fragments) in the final state as well as the momentum transfer in the collision can be exactly determined. In an experiment, however, these quantities can only be measured approximately.

In an 'ideal' experiment, one would fulfill two requirements: (i) to work with a high quality (monochromatic) beam of projectiles; and (ii) to measure the momenta of all particles with an accuracy sufficient to resolve the allowed momentum bands along the x and z directions which—according to Equation (8)—are given by $-P_a^i\, b/2D \leq \mathcal{P}_x \leq P_a^i\, b/2D$ and $P_a^i\, d\, n/D - P_a^i\, a/2D \leq \mathcal{P}_z \leq P_a^i\, d\, n/D + P_a^i\, a/2D$, respectively.

There seems to be no big problem with fulfilling the requirement (i): for instance, the typical energy spread of $10 - 100$ keV/u ions can be optimized to a few eV meeting the monochromatic beam criteria.

The requirement (ii) is more severe, however, it can be somewhat softened since one does not need to measure all momenta with the same (high) accuracy.

Indeed, in the case of elastic scattering (considered in subsection III.A), the necessary accuracy $\Delta P^f_{a,z}$ in the determination of the momentum component $P^f_{a,z}$ is set by the condition $\Delta P^f_{a,z} < P^i_a d/D$ which can be quite strict (for instance, $\Delta P^f_{a,z} < 0.1$ a.u. in the example considered in Figure 2). However, since the cross-section displayed in Figure 2 was obtained by integrating over $P^f_{a,x}$ and $P^f_{a,y}$, there is no such restriction on the accuracy of the determination of the corresponding momentum components.

In the case of ionization, discussed in subsection III.B, the restrictions on the accuracy in measuring the momenta follow from the inequality $B^- \leq (k_z - v)^2 + k^2_\perp \leq B^+$ ($B^\pm = v^2 - 2|\varepsilon_i| + 2\,v\,P_{R,z} + 2\,v\,P^i_a\,\frac{d}{D}\,n \pm v\,P^i_a\,\frac{a}{D}$). If we suppose that the electron momenta can be measured with much better accuracy than those of the recoil ion (like, e.g., it is the case with cold target recoil ion momentum spectroscopy (COLTRIMS) techniques [35]) then the uncertainty $\Delta P_{R,z}$ will be determined by the condition $\Delta P_{R,z} < P^i_a d/D$ which can be quite severe ($\Delta P_{R,z} < 0.05$ a.u. in the example considered in Figure 3). The spectrum shown in Figure 3 follows from the cross-section (10) which was obtained by integrating over the components $P_{R,x}$ and $P_{R,y}$ of the target recoil ion. Therefore, there is no such restriction on the accuracy of measuring these momentum components. Additionally, since the components q_x and q_y of the momentum transfer in the collision do not enter the term $\sum_n F^2_a(B_n)$ in Equation (10) determining the interference pattern in Figure 3 (note that this also remains true in calculations employing the continuum-distorted-wave eikonal-initial-state approach), there are also no strict restrictions on the accuracy of measuring these components in an experiment.

By summarizing the above discussion, we can conclude that the requirement (ii) is fulfilled if the conditions $\Delta P^f_{a,z} < P^i_a d/D$ and $\Delta k_{z,tr} < \Delta P_{R,z} < P^i_a d/D$ are met for the elastic scattering and ionization, respectively, where Δk_z and Δk_{tr} are uncertainties in the measured components of the electron momentum.

These conditions seem to be quite challenging for experiments which employ the COLTRIMS techniques. Indeed, in such experiments, helium targets have momenta that are substantially less than the value $P^i_a = 50$ a.u. used to obtain the results shown in Figure 3. Smaller P^i_a reduce the size and thickness of the momentum rings in Figure 3, setting an even stronger requirement on the accuracy in the momentum determination. To prepare the initial target moment of $P^i_a \sim 50$–100 a.u., one could use heavier targets (e.g., Ar or Xe). However, for heavy targets, the accuracy of the momenta determination is usually of the order of a few atomic units for a reaction microscope equipped with the room-temperature super-sonic gas jet, which is far away from the value of $\lesssim$0.1 a.u. necessary to resolve the structures in Figures 2 and 3. To reach a much better accuracy, a reaction microscope with a precooling super-sonic gas jet can be envisaged.

To conclude this subsection, we note that the requirements on the accuracy in the determination of the final momenta in the collision can be greatly softened if, instead of the ionization of target atoms, a closely related process of projectile electron loss is considered. In such a case, a structured projectile (e.g., He^+) passes through a macroscopic grating and, due to much higher incident momenta p^i_p, the allowed momentum bands, $p^i_p\,d\,n/D - p^i_p\,a/2D \leq \mathcal{P}_z \leq p^i_p\,d\,n/D + p^i_p\,a/2D$ along the direction of the macroscopic grating will be much broader. For instance, for 25–100, keV/u He^+ ions passed through a grating with $a \simeq b \simeq 0.1$ mm, one obtains $p^i_p\,a/D \simeq 3.5 - 7$ a.u. at $D = 200$ mm which means that the interference structures can be resolved even if the accuracy of the momentum determination is of the order of a few atomic units.

4. Conclusions

In conclusion, due to a regular space structure acquired by the wave function of an atom passed through a macroscopic diffraction grating, this atom can itself be regarded as a diffraction grating. Compared to macroscopic gratings and even to microscopic gratings represented by molecules, this type is qualitatively different since it consists of just a single

atom. The role of the structured "real matter" in the former ones is now mimicked by the structured probability amplitude (wavefunction).

We considered two- and three-particle interference effects appearing when such an atomic quantum grating is probed by collisions with point-like charged projectiles. These are due to the coherent addition of the contributions of different 'slits' of the atomic grating to the transition amplitude (the superposition principle) and the quantum entanglement of the involved particles. These effects very clearly manifest themselves in both elastic and ionizing collisions.

In particular, interesting patterns arise in the spectra of electrons ejected in collisions with ions in the kinematic range where there is a 'confluence' of the binary-encounter emission and electron capture to the projectile continuum. In such a case, a pronounced interference structure appears in the emission spectrum whose shape is extremely sensitive to the magnitude of the collision velocity. This point might potentially be exploited for a precise determination of this velocity.

Author Contributions: B.N., S.Z., X.M. and A.B.V. contributed equally to this research. All authors have read and agreed to the published version of the manuscript.

Funding: This research was funded by the National Key Research and Development Program of China (Grant No. 2017YFA0402300) and via the CAS President's International Fellowship Initiative.

Data Availability Statement: Not applicable.

Acknowledgments: We acknowledge the support from the National Key Research and Development Program of China (Grant No. 2017YFA0402300), the CAS President's International Fellowship Initiative. We thank Reinhard Dörner and Carsten Müller for useful discussions.

Conflicts of Interest: The authors declare no conflict of interest.

References

1. de Broglie, L. Louis de Broglie's conception of physics. *Ann. Found.* **1992**, *17*, 22.
2. Davisson, C.J.; Germer, L.H. Diffraction of Electrons by a Crystal of Nickel. *Phys. Rev.* **1927**, *30*, 705–740. [CrossRef]
3. Thomson, G.P. Experiments on the Diffraction of Cathode Rays. *Proc. R. Soc.* **1928**, *A117*, 600.
4. Fein, Y.Y.; Geyer, F.; Zwick, P.; Kialka, F.; Pedalino, S.; Mayor, M.; Gerlich, S.; Arndt, M. Quantum superposition of molecules beyond 25 kDa. *Nat. Phys.* **2019**, *15*, 1242–1245. [CrossRef]
5. Young, T. Philosophical Transactions. 24 November 1803. Available online: https://royalsocietypublishing.org/doi/pdf/10.1098/rstl.1804.0001?download=true (accessed on 19 September 2022).
6. Tuan, T.F.; Gerjuoy, E. Charge Transfer in Molecular Hydrogen. *Phys. Rev.* **1960**, *117*, 756–763. [CrossRef]
7. Cohen, H.; Fano, U. Interference in the Photo-Ionization of Molecules. *Phys. Rev.* 1966, *150*, 30–33. [CrossRef]
8. Lindner, F.; Schätzel, M.G.; Walther, H.; Baltuška, A.; Goulielmakis, E.; Krausz, F.; Milošević, D.B.; Bauer, D.; Becker, W.; Paulus, G.G. Attosecond Double-Slit Experiment. *Phys. Rev. Lett.* **2005**, *95*, 040401. [CrossRef] [PubMed]
9. Fernández, J.; Fojón, O.; Palacios, A.; Martín, F. Interferences from Fast Electron Emission in Molecular Photoionization. *Phys. Rev. Lett.* **2007**, *98*, 043005. [CrossRef]
10. Akoury, D.; Kreidi, K.; Jahnke, T.; Weber, T.; Staudte, A.; Schöffler, M.; Neumann, N.; Titze, J.; Schmidt, L.P.H.; Czasch, A.; et al. The Simplest Double Slit: Interference and Entanglement in Double Photoionization of H_2. *Science* **2007**, *318*, 949. [CrossRef]
11. Zimmermann, B.; Rolles, D.; Langer, B.; Hentges, R.; Braune, M.; Cvejanovic, S.; Geßner, O.; Heiser, F.; Korica, S.; Lischke, T.; et al. Localization and loss of coherence in molecular double-slit experiments. *Nat. Phys.* **2008**, *4*, 649. [CrossRef]
12. Kreidi, K.; Akoury, D.; Jahnke, T.; Weber, T.; Staudte, A.; Schöffler, M.; Neumann, N.; Titze, J.; Schmidt, L.P.H.; Czasch, A.; et al. Interference in the Collective Electron Momentum in Double Photoionization of H_2. *Phys. Rev. Lett.* **2008**, *100*, 133005. [CrossRef] [PubMed]
13. Lin, C.D.; Le, A.T.; Chen, Z.; Morishita, T.; Lucchese, R. Strong-field rescattering physics—Self-imaging of a molecule by its own electrons. *J. Phys. B* **2010**, *43*, 122001. [CrossRef]
14. Cherepkov, N.A.; Semenov, S.K.; Schöffler, M.S.; Titze, J.; Petridis, N.; Jahnke, T.; Cole, K.; Schmidt, L.P.H.; Czasch, A.; Akoury, D.; et al. Auger decay of $1\sigma_g$ and $1\sigma_u$ hole states of the N_2 molecule. II. Young-type interference of Auger electrons and its dependence on internuclear distance. *Phys. Rev. A* **2010**, *82*, 023420. [CrossRef]
15. Milne-Brownlie, D.S.; Foster, M.; Gao, J.; Lohmann, B.; Madison, D.H. Young-Type Interference in $(e, 2e)$ Ionization of H_2. *Phys. Rev. Lett.* **2006**, *96*, 233201. [CrossRef]
16. Stolterfoht, N.; Sulik, B.; Hoffmann, V.; Skogvall, B.; Chesnel, J.Y.; Rangama, J.; Frémont, F.; Hennecart, D.; Cassimi, A.; Husson, X.; et al. Evidence for Interference Effects in Electron Emission from H_2 Colliding with 60MeV/u Kr^{34+} Ions. *Phys. Rev. Lett.* **2001**, *87*, 023201. [CrossRef]

17. Misra, D.; Kadhane, U.; Singh, Y.P.; Tribedi, L.C.; Fainstein, P.D.; Richard, P. Interference Effect in Electron Emission in Heavy Ion Collisions with H_2 Detected by Comparison with the Measured Electron Spectrum from Atomic Hydrogen. *Phys. Rev. Lett.* **2004**, *92*, 153201. [CrossRef]
18. Dimopoulou, C.; Moshammer, R.; Fischer, D.; Höhr, C.; Dorn, A.; Fainstein, P.D.; Crespo López Urrutia, J.R.; Schröter, C.D.; Kollmus, H.; Mann, R.; et al. Breakup of H_2 in Singly Ionizing Collisions with Fast Protons: Channel-Selective Low-Energy Electron Spectra. *Phys. Rev. Lett.* **2004**, *93*, 123203. [CrossRef]
19. Schmidt, H.T.; Fischer, D.; Berenyi, Z.; Cocke, C.L.; Gudmundsson, M.; Haag, N.; Johansson, H.A.; Källberg, A.; Levin, S.B.; Reinhed, P.; et al. Evidence of Wave-Particle Duality for Single Fast Hydrogen Atoms. *Phys. Rev. Lett.* **2008**, *101*, 083201. [CrossRef]
20. Schmidt, L.P.H.; Schössler, S.; Afaneh, F.; Schöffler, M.; Stiebing, K.E.; Schmidt-Böcking, H.; Dörner, R. Young-Type Interference in Collisions between Hydrogen Molecular Ions and Helium. *Phys. Rev. Lett.* **2008**, *101*, 173202. [CrossRef]
21. Alexander, J.S.; Laforge, A.C.; Hasan, A.; Machavariani, Z.S.; Ciappina, M.F.; Rivarola, R.D.; Madison, D.H.; Schulz, M. Interference effects due to projectile target nucleus scattering in single ionization of H_2 by 75−keV proton impact. *Phys. Rev. A* **2008**, *78*, 060701(R). [CrossRef]
22. Misra, D.; Schmidt, H.T.; Gudmundsson, M.; Fischer, D.; Haag, N.; Johansson, H.A.; Källberg, A.; Najjari, B.; Reinhed, P.; Schuch, R.; et al. Two-Center Double-Capture Interference in Fast $\mathbf{He}^{2+} + \mathbf{H}_2$ Collisions. *Phys. Rev. Lett.* **2009**, *102*, 153201. [CrossRef] [PubMed]
23. Voitkiv, A.B.; Najjari, B.; Fischer, D.; Artemyev, A.N.; Surzhykov, A. Young-Type Interference in Projectile-Electron Loss in Energetic Ion-Molecule Collisions. *Phys. Rev. Lett.* **2011**, *106*, 233202. [CrossRef]
24. Zhang, S.F.; Fischer, D.; Schulz, M.; Voitkiv, A.B.; Senftleben, A.; Dorn, A.; Ullrich, J.; Ma, X.; Moshammer, R. Two-Center Interferences in Dielectronic Transitions in $H_2^+ +$ He Collisions. *Phys. Rev. Lett.* **2014**, *112*, 023201. [CrossRef]
25. Gao, Y.; Zhang, S.F.; Zhu, X.L.; Guo, D.L.; Schulz, M.; Voitkiv, A.B.; Zhao, D.M.; Hai, B.; Zhang, M.; Zhang, R.T.; et al. Probing scattering phases via two-center interferences in collisions of He^{2+} on CO. *Phys. Rev. A* **2018**, *97*, 020701(R). [CrossRef]
26. Zhang, S.F.; Najjari, B.; Ma, X.; Voitkiv, A.B. Photo ionization of an atom passed through a diffraction grating. *arXiv* **2020**, arXiv:2008.02453.
27. Zhang, S.F.; Najjari, B.; Ma, X. Photoionization of a quantum grating formed by a single atom. *J. Phys. B* **2021**, *54*, 15LT01. [CrossRef]
28. Horne, M.A.; Shimony, A.; Zeilinger, A. Two-particle interferometry. *Phys. Rev. Lett.* **1989**, *62*, 2209. [CrossRef]
29. Pan, J.W.; Chen, Z.-B.; Lu, C.Y.; Weinfurter, H.; Zeilinger, A.; Zukowski, M. Multiphoton entanglement and interferometry. *Rev. Mod. Phys.* **2012**, *84*, 777. [CrossRef]
30. Lopes, R.; Imanaliev, A.; Aspect, A.; Cheneau, M.; Boiron, D.; Westbrook, C.I. Atomic Hong–Ou–Mandel experiment. *Nature* **2015**, *520*, 66. [CrossRef]
31. Waitz, M.; Metz, D.; Lower, J.; Schober, C.; Keiling, M.; Pitzer, M.; Mertens, K.; Martins, M.; Viefhaus, J.; Klumpp, S.; et al. Two-Particle Interference of Electron Pairs on a Molecular Level. *Phys. Rev. Lett.* **2016**, *117*, 083002. [CrossRef]
32. Fischer, D.; Voitkiv, A.B.; Moshammer, R.; Ullrich, J. Three-body momentum exchange in singly ionizing 2-MeV/u C^{6+}-helium collisions. *Phys. Rev. A* **2003**, *68*, 032709. [CrossRef]
33. Macek, J.H.; Manson, S.T. *Springer Handbook on Atomic, Molecular and Optical Physics*; Springer: Berlin, Germany, 2006; Chapter 53.
34. Crothers, D.S.F.; McCann, J. Ionisation of atoms by ion impact. *J. Phys. B* **1983**, *16*, 3229. [CrossRef]
35. Ullrich, J.; Moshammer, R.; Dorn, A.; Dörner, R.; Schmidt, L.P.H.; Schmidt-Böcking, H. Recoil-ion and electron momentum spectroscopy: Reaction-microscopes. *Rep. Prog. Phys.* **2003**, *66*, 1463. [CrossRef]